nature immunology

© 2007 Nature Publishing Group http://www.nature.com/natureimmunology

A structural basis for complement inhibition by *Staphylococcus aureus*

Michal Hammel[1,3,4], Georgia Sfyroera[2,4], Daniel Ricklin[2], Paola Magotti[2], John D Lambris[2] & Brian V Geisbrecht[1]

To provide insight into bacterial suppression of complement-mediated immunity, we present here structures of a bacterial complement inhibitory protein, both free and bound to its complement target. The 1.25-Å structure of the complement component C3–inhibitory domain of *Staphylococcus aureus* extracellular fibrinogen-binding protein (Efb-C) demonstrated a helical motif involved in complement regulation, whereas the 2.2-Å structure of Efb-C bound to the C3d domain of human C3 allowed insight into the recognition of complement proteins by invading pathogens. Our structure-function studies provided evidence for a previously unrecognized mode of complement inhibition whereby Efb-C binds to native C3 and alters the solution conformation of C3 in a way that renders it unable to participate in successful 'downstream' activation of the complement response.

As a central component of human immunity, the complement system is composed of a series of exquisitely regulated secreted and cell surface–exposed proteins that serve as a powerful, acute effector mechanism capable of dealing with foreign materials directly or recruiting 'downstream' defense mechanisms of the body. Inappropriate activation of the complement system is the cause of considerable injury and has been linked to several autoimmune disorders; therapeutic inhibition of the complement system has been suggested as an approach for treating many such diseases[1–3]. In steady-state physiological conditions, activation of the complement system is strictly regulated by a series of 'regulator of complement activation' (RCA) proteins. Among these are soluble serum proteins, such as factor H and complement component 4b (C4b)–binding protein, as well as the membrane-bound proteins complement receptor 1 (CD35), membrane cofactor protein (CD46) and decay-accelerating factor (CD55). In general, RCA proteins suppress the activation of C3 and C4 by dissociating the subunits of C3 and/or C5 convertases or by acting as cofactors for factor I–dependent cleavage of C3b and/or C4b[1–3]. Detailed understanding of the molecular mechanisms underlying RCA protein-mediated control of complement activation would be useful for the rational design of potent complement inhibitors[1–3]. Unfortunately, limited structural information on RCA-ligand complexes has hindered understanding of the molecular-recognition mechanisms of this class of proteins.

Staphylococcus aureus is a persistent human pathogen that is responsible for a wide range of diseases that vary in both clinical presentation and severity. Perhaps more so than any other bacterial pathogen, *S. aureus* has evolved the ability to adapt to distinct microenvironments in the human body. Although the diverse functionality of its surface-bound adhesins (microbial surface components recognizing adhesive matrix molecules[4]) contributes to that ability, present models also suggest that the success of this organism as a pathogen can be predicated by its capacity to manipulate and evade multiple host immune responses[5–9].

The circulating complement system is a chief target of virulence factors produced by many pathogens[10]. Because it is central in the amplification of all three complement pathways (classical, alternative and lectin-mediated activation), C3 represents a particularly likely target for organisms seeking to inhibit or modulate the essential complement response[7,11]. *S. aureus* stimulates all three pathways of the complement system[12–16], and mice depleted of complement by treatment with cobra venom factor have been found to be more susceptible to *S. aureus*–induced septicemia than are untreated mice[17]. Those results indicate that complement serves a principal function in the global immune response against *S. aureus* infection and suggest that the bacterium probably produces complement inhibitors that mimic the function of RCA proteins[7]. Indeed, conditioned *S. aureus* culture medium contains at least one C3b-binding protein, which has been identified as the 15.6-kilodalton extracellular fibrinogen-binding protein (Efb)[7]. Functional analysis has shown that recombinant Efb binds to the thioester-containing C3d domain of C3b and inhibits the deposition of C3b onto sensitized surfaces[7,8] and that *S. aureus* strains incapable of expressing Efb are less virulent than a wild-type strain in a mouse model of wound healing[18]. Thus, attenuation of the complement response by *S. aureus* seems to be a critical mechanism of immunosuppression that is advantageous to its function as a human

[1]Division of Cell Biology and Biophysics, School of Biological Sciences, University of Missouri at Kansas City, Kansas City, Missouri 64110, USA. [2]Department of Pathology and Laboratory Medicine, University of Pennsylvania, Philadelphia, Pennsylvania 19104, USA. [3]Present address: Advanced Light Source, Lawrence Berkeley Laboratory, Berkeley, California 94720, USA. [4]These authors contributed equally to this work. Correspondence should be addressed to B.V.G. (geisbrechtB@umkc.edu).

Received 14 September 2006; accepted 9 February 2007; published online 11 March 2007; doi:10.1038/ni1450

© 2007 Nature Publishing Group http://www.nature.com/natureimmunology

Table 1 Data collection and refinement statistics

	Efb-C[a]	Efb-C–C3d
Data collection		
Space group		$P4_1$
Unit cell dimensions (Å)		$a = b = 90.9$; $c = 122.2$
Molecule/ASU		2
Resolution limits (Å)		50–2.2
Completeness (%)		98.8 (83.4)
Total reflections		244,752
Unique reflections		49,718
R_{merge} (%)[b]		9.2 (47.3)
$I/\sigma I$		12.7 (1.8)
Refinement statistics		
R_{cryst}/R_{free} (%)[c]	21.1/21.8	18.1/23.1
r.m.s. deviation from ideality		
Bond length (Å)	0.006	0.024
Bond angle (°)	0.93	1.87
Dihedral angle (°)	18.7	18.5
Ramachandran core (%)		
Disallowed	96.5 (0)	93.4 (0)
B values		
Average B factor (Å^2)	19.0	43.5
r.m.s. deviation of B factor (Å^2)	1.2	11.4
Proteins atoms modeled	987	5,674
Ordered solvent molecules	155	317

Numbers in parentheses are for the shell of highest resolution (2.28–2.20 Å). ASU, asymmetric unit.
[a]Data collection and X-ray diffraction analysis of Efb-C has been published before[34]. [b]$R_{merge} = \Sigma_h\Sigma_i|I_i(h) - \langle I(h)\rangle| / \Sigma_h\Sigma_i I_i(h)$, where '$I_i(h)$' is the 'ith' measurement of reflection 'h' and '$\langle I(h)\rangle$' is a weighted mean of all measurements of 'h'. [c]$R = \Sigma_h|F_o(h) - F_c(h)| / \Sigma_h|F_o|$, where F_o and F_c are the observed and calculated structure factors, respectively. R_{cryst} and R_{free} were calculated from the working and test reflection sets, respectively. The test set constituted 5% of the total reflections not used in refinement.

pathogen. To provide structural and mechanistic insight into bacterial suppression of complement-mediated innate immunity, we present here crystal structures of the C3-binding domain of Efb (Efb-C), both free and bound to its human complement target, the C3d domain of human C3. In addition, we report a series of structure-function studies that provide evidence for a previously unrecognized mode of complement inhibition.

RESULTS

Structures of Efb-C alone and bound to C3d

To gain structural insight into the molecular recognition of RCA proteins and their involvement in complement cascade inhibition by *S. aureus*, we determined the crystal structure of Efb-C using multi-wavelength anomalous diffraction data collected from crystals of selenomethionyl-substituted protein and refined to limiting resolution of 1.25 Å with R_{cryst} and R_{free} values of 21.1% and 21.8%, respectively (**Table 1**). The overall dimensions of Efb-C were approximately 40 × 25 × 20 Å, with the N-terminal α1 helix (K106–H125) connected through a short loop to the α2 helix (V127–L139), followed by the C-terminal α3 helix (K145–Q161), and terminating in a random coil conformation (G162–R165; **Fig. 1a**). All three helices were packed in a canonical three-helix bundle fold, with most of the nonpolar side chains directed inward; however, there was an obvious preponderance of solvent-exposed basic residues in Efb-C (**Fig. 1b**).

All known examples of complement-regulatory proteins, including factor H, its viral homolog vaccinia virus complement-control protein, membrane cofactor protein, decay-accelerating factor, complement receptor 1 and C4b-binding protein, contain a short consensus repeat or complement-control protein β-type fold[2]. In contrast, the Efb-C structure was entirely helical and therefore defined a previously unrecognized fold class for complement regulatory proteins. However, this type of all-helical structure is not unprecedented among extracellular staphylococcal proteins, as the Efb-C structure is reminiscent of *S. aureus* protein A modules (**Supplementary Fig. 1** online). Nevertheless, the topological arrangement of the helices in Efb-C is distinct from that in protein A, so an evolutionary relationship between these two classes of virulence factors is unlikely.

To better understand the nature of Efb-C3 interactions and complement component recognition, we determined the crystal structure of Efb-C bound to recombinant C3d. We refined the Efb-C–C3d structure to a limiting resolution of 2.2 Å with R_{cryst} and R_{free} values of 18.1% and 23.1%, respectively (**Fig. 2a** and **Table 1**). A single Efb-C molecule bound to C3d in the complex, and comparison of Efb-C in its free versus bound state showed minimal structural changes. In particular, there was ordered character up to residue T101 of Efb-C when it was bound to C3d, a finding that most likely reflected stabilization of the N-terminal α1 helix in Efb-C through interaction with C3d. Overall, 61 of 65 residues aligned within 2.5 Å and an r.m.s. deviation of 0.47 Å when we compared the free and bound states of Efb-C. This suggested that the C3d binding site on Efb-C is preformed.

In the 'co-crystal', C3d adopted its canonical dome-shaped helical structure[19] and a single Efb-C molecule was present at the periphery of the conserved acidic pocket comprising residues D1029, E1030, E1032, D1156, E1159 and E1160 on the concave surface of C3d (**Fig. 2b** and **Supplementary Fig. 2** online). Most of the contacting residues were donated from Efb-C helix α2 (H130, R131, K135 and N138), although side chains from helices α1 (K106 and K110) and α3 (K148) also seemed capable of serving a minor function in forming the Efb-C–C3d complex. In contrast to the interacting residues in Efb-C, the C3d residues at the complex interface were separate in the sequence but came together in the folded protein. In particular, residues from the

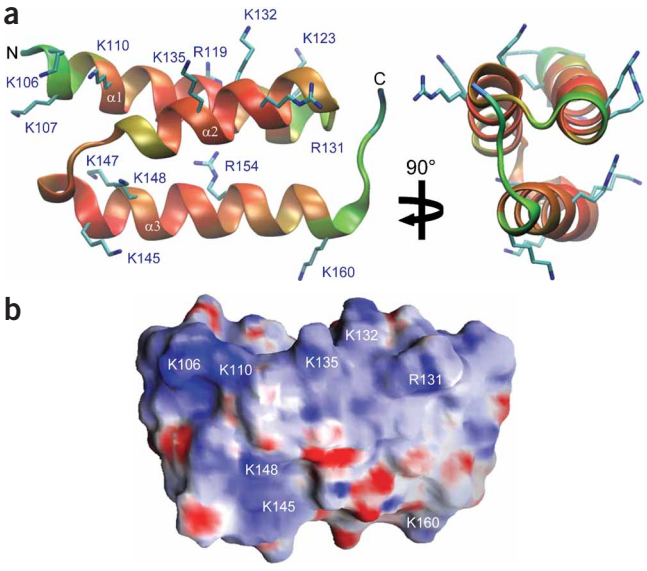

Figure 1 Crystal structure of Efb-C at 1.25 Å. (**a**) Two orthogonal views of the refined Efb-C structure (ribbons). Refined temperature factors: blue, about 28 Å^2; red, about 10 Å^2. (**b**) Surface charge distribution. Blue, areas with +15 electrons per angstrom; red, areas with –15 electrons per angstrom. Protein termini and positions of surface-exposed basic residues are labeled.

© 2007 Nature Publishing Group http://www.nature.com/natureimmunology

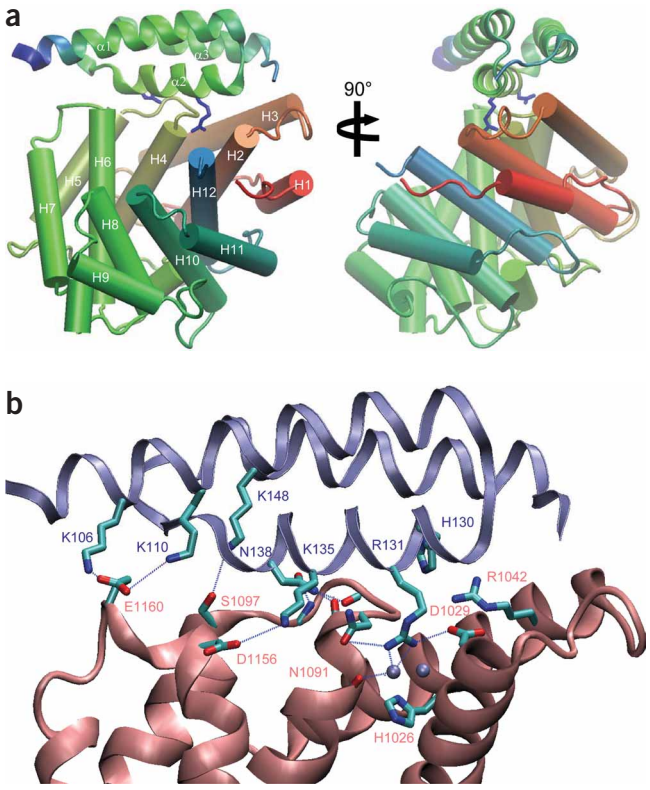

Figure 2 Crystal structure of the Efb-C–C3d complex at 2.2 Å. (**a**) Two orthogonal views of the Efb-C–C3d complex structure. C3d is presented from the N terminus (red) to the C terminus (blue) with helices (cylinders) H1–H12 labeled. Efb-C (ribbon) colors are according to the temperature factor at each position: blue, about 85 Å^2; green, about 40 Å^2; helices α1, α2 and α3 are labeled. Blue 'stick models' are residues R131 and N138 of Efb-C. (**b**) Interface of Efb-C (blue) and C3d (red). Residues involved in protein-protein contacts (stick models) are labeled. Silver spheres, two structural water molecules involved in the R131 contact; dashed lines, hydrogen bond contacts.

loops connecting the H2-H3, H4-H5 and H6-H7 helices formed specific contacts with Efb-C. The Efb-C–C3d interface demonstrated excellent shape complementarity with a relatively large buried surface area of 1,967 Å^2 that accounted for 44% of the available Efb-C surface. This surface compatibility was particularly notable for residue R131 of Efb-C, which was tucked deeply within a solvent-lined pocket of C3d comprising residues H1026, D1029, N1091 and L1092 (**Fig. 2b**). Closer inspection of the intermolecular hydrogen bonds also showed an intricate network between N138 of Efb-C and the main-chain atoms of residues V1090, I1093 and I1095 that formed the H4-H5 loop of C3d (**Fig. 2b**).

Efb-C-induced C3 conformational change

Studies have indicated that Efb-C is both necessary and sufficient to block complement pathway activation[7,8], and the crystal structures presented here suggested that such inhibition results from the ability of Efb-C to form a specific, high-affinity complex with the C3d domain of C3. To investigate the biochemical nature of the Efb-C3 complex more closely, we used isothermal titration calorimetry to examine the binding of full-length Efb, Efb-N (the N-terminal region of Efb) and Efb-C, as well as two Efb-C mutants, to C3d (**Fig. 3a**). Efb and Efb-C had high-affinity, 1:1 binding to C3d, based on their equilibrium dissociation constant values of 4 ± 2 nM and 2 ± 1 nM, respectively; we obtained similar values for enthalpic contribution: –9.0 kcal/mol and –8.5 kcal/mol for full-length Efb and Efb-C, respectively. Our results were in agreement with published studies demonstrating that Efb-C is necessary and sufficient for binding to C3d[8] and that Efb-N contributes only the fibrinogen-binding activity of Efb, as the truncated Efb-N protein had no measurable affinity for C3d in this assay[8]. We then assessed the C3d-binding properties of two site-directed double mutants of Efb-C using the same assay: Efb-C-(RANA), with R131A and N138A substitutions, and Efb-C-(RENE), with R131E and N138E substitutions (**Fig. 3a**). In both cases, the results of these studies supported the findings of Efb-C–C3d interactions determined from the crystal structure, as neither double mutant had detectable binding to C3d despite the fact that each was structurally intact (data not shown and **Supplementary Fig. 3** online). The finding that Efb-C-(RANA) demonstrated no binding to C3d emphasized the importance of the specific noncovalent interactions formed by both R131 and N138 (**Fig. 2b**) and suggested that the contacts formed between the other residues at the Efb-C–C3d interface were insufficient to drive complex formation.

The site-directed mutagenesis studies presented above confirmed the importance of both R131 and N138 in forming the Efb-C–C3d complex (**Fig. 3a**) and identified Efb-C mutants incapable of binding to C3d. To understand the function of the Efb-C–C3d complex in complement inhibition more thoroughly, we measured the activity of Efb, Efb-C and the nonfunctional Efb-C-(RENE) mutant in a series of quantitative, functional assays that monitored the generation and surface deposition of C3b through either the classical or alternative pathway (**Fig. 3b** and data not shown). These experiments suggested that the inhibitory properties of Efb are directly related to C3d binding, as Efb and Efb-C had essentially identical activities, whereas Efb-C-(RENE) had no activity in either assay. Furthermore, whereas a

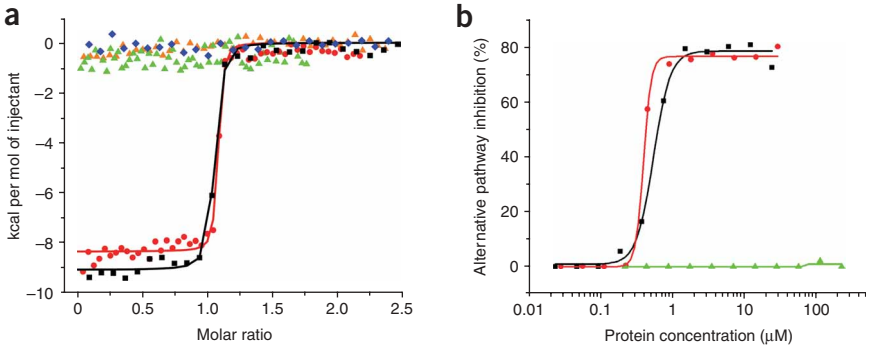

Figure 3 Inhibition of C3 activation requires binding of Efb to the C3d domain. (**a**) Thermodynamics of the Efb-C3d interaction, assessed quantitatively by isothermal titration calorimetry and site-directed mutagenesis. Data are fitted isothermal titration calorimetry binding curves for titrations of Efb (black), Efb-N (blue), Efb-C (red) and double-mutants Efb-C-(RANA) (orange) and Efb-C-(RENE) (green), diluted into a solution of recombinant C3d. (**b**) ELISA of the ability of various concentrations of Efb (black), Efb-C (red) and Efb-C-(RENE) (green) to inhibit the alternative pathway of complement activation. Data are one representative of two (**a**) or three (**b**) experiments.

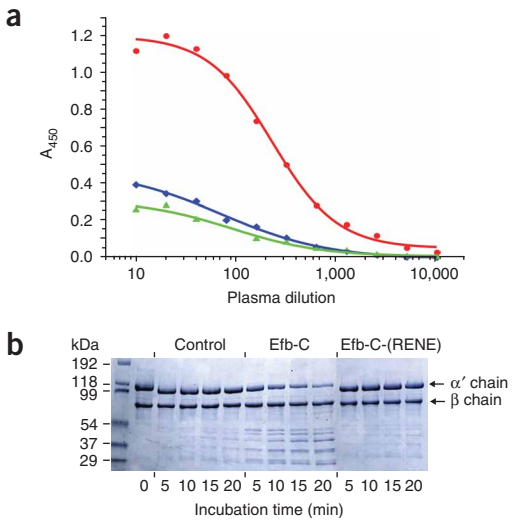

Figure 4 Structural basis of complement inhibition by Efb-C. (**a**) Capture ELISA of the conformational changes of plasma C3. Diluted plasma containing EDTA (for blockade of the complement cascade) was incubated for 1 h at 37 °C with Efb-C, Efb-C-(RENE) or buffer alone, followed by 'capture' on ELISA plates coated with monoclonal antibody C3-9. Bound C3 was detected with antibody to C3a and horseradish peroxidase–conjugated goat antibody to rabbit. A_{450}, absorbance at 450 nm. (**b**) Protease-sensitivity assay of the change in C3 conformation induced by Efb-C binding. Purified C3 was incubated with Efb-C, Efb-C-(RENE) or buffer alone (Control) and was subjected to limiting proteolysis by 0.1% (wt/wt) trypsin. Aliquots from each reaction were removed at 5, 10, 15 and 20 min and were separated by SDS-PAGE, then were compared, by Coomassie staining of the gel, with a control sample of C3 incubated without trypsin (lane 2; 0 min). Control, C3 in buffer with trypsin. Figure contrast has been increased uniformly to enhance band visualization. Additional control digestions are in **Supplementary Figure 4**. Data are one representative of three experiments.

50-fold molar excess of Efb over C3 was needed to achieve an half-maximal inhibitory concentration for the classical pathway, both Efb and Efb-C reached the half-maximal inhibitory concentration (560 nM and 410 nM for Efb and Efb-C, respectively) when essentially equimolar with C3 in the alternative pathway assay. This indicated that the principal effect of Efb occurs through blockade of the alternative pathway; the observed effect on the classical pathway most likely reflected Efb-mediated inhibition of the alternative pathway self-amplification loop, which contributes most of the C3b generated by the classical pathway[20].

To further define the functional basis for Efb-mediated inhibition of the alternative pathway, we incubated the C3 in human plasma with Efb-C, Efb-C-(RENE) or buffer alone and assessed the reactivity of each sample over a 1,000-fold dilution range with a well established panel of monoclonal antibodies[21] that bind in a way specific for particular compositions and conformations of C3 and/or the various intermediates of its activation and degradation pathways. Treatment of plasma with Efb-C resulted in a considerable increase in the reactivity of bound C3 with monoclonal antibody C3-9, which detects a neoantigen that becomes exposed during activation of C3 to hydrolyzed C3 ($C3(H_2O)$) and C3b[22]. The finding that C3 captured in this way was recognized by both C3a- and C3b-specific antibodies (**Fig. 4a** and data not shown) throughout the entire dilution series indicated that C3 bound to Efb-C was not being processed into C3b but that Efb-C binding altered the conformation of C3, resulting in increased exposure of the C3-9-specific epitope.

Protease-sensitivity assays have long been used as a biochemical probe to assess the folding state and structure of proteins. Limiting proteolysis by trypsin showed that C3 bound to Efb-C was rapidly processed into a series of lower-molecular-weight fragments, whereas only small amounts of the fragments were present in samples containing equal quantities of Efb-C-(RENE) or buffer alone, even after prolonged exposure to trypsin (**Fig. 4b** and **Supplementary Fig. 4** online). We noted a similar effect in plasma samples in which complement activation was blocked by the addition of EDTA. Here, the addition of Efb-C resulted in sensitivity of C3 to proteolysis that was not detected for either Efb-C-(RENE) or untreated controls (**Supplementary Fig. 5** online). These results collectively indicated that Efb-C binding resulted in a C3 conformational change that exposed an epitope found in $C3(H_2O)$ and that was unable to participate in 'downstream' complement activation.

Efb-C binding 'preference' for native C3

The crystal structures of C3, C3b and C3c[23,24], along with considerable biochemical data, have demonstrated that activation of C3 to C3b is accompanied by substantial conformational changes[2,25–27]. Such conversions lead to the exposure of previously hidden binding sites and to changes in affinity for an array of receptors and regulatory proteins in C3b relative to C3, which has few physiological ligands in its native state[2]. Given that knowledge, the Efb-C-induced conformational

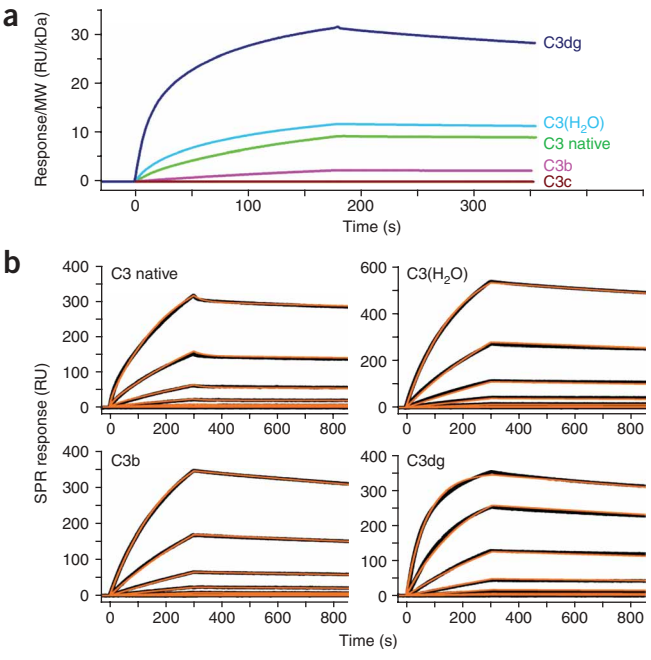

Figure 5 Efb-C binds to native forms of C3. (**a**) SPR ranking. Efb-C was immobilized on the surface of a sensor chip and C3 intermediates were injected at a constant concentration of 200 nM. Each binding curve was normalized by division of the SPR signal by the molecular weight (MW, in kilodaltons (kDa)) of the injected protein, as the SPR response is dependent on analyte mass. (**b**) SPR kinetic profiles of selected C3 fragments binding to Efb-C. The processed binding curves for each fragment (black lines) were fitted to kinetic models (brown lines) describing either 1:1 Langmuir binding ($C3(H_2O)$, C3b and C3dg) or surface heterogeneity (native C3). Kinetic rate constants derived from these results are in **Table 2**. RU, resonance units. Data are one representative of three (**a**) or two to three (**b**) experiments.

© 2007 Nature Publishing Group http://www.nature.com/natureimmunology

Table 2 SPR kinetic profiles of C3 fragments binding to Efb-C

Target	Analyte	k_{on} (10^4 $M^{-1}s^{-1}$)	k_{off} (10^{-4} s^{-1})	K_d (nM)
Efb-C	C3 native[a]	3.60 ± 0.03	0.99 ± 0.19	2.8 ± 0.5
	$C3(H_2O)$	8.89 ± 0.87	1.69 ± 0.14	1.9 ± 0.0
	C3b	2.39 ± 0.13	2.09 ± 0.01	8.8 ± 0.5
	C3dg	28.44 ± 11.89	2.18 ± 0.42	0.8 ± 0.1

All analytes were injected over immobilized Efb-C as threefold linear dilution series (200–0.9 nM for C3b; 67–0.09 nM for other analytes). Data were fit to either a 1:1 Langmuir ($C3(H_2O)$, C3b and C3dg) or a surface heterogeneity binding model (C3 native and are presented as ± s.d.). k_{on}, association rate constant; k_{off}, dissociation rate constant; K_d, dissociation constant.
[a]Kinetic rate constants of the primary binding site (about 90% of the calculated maximum binding response).

changes in C3 identified above suggested that Efb-C may also bind differently to C3 and its various intermediates that represent different states of its activation pathway. To test that hypothesis, we immobilized Efb-C on a surface plasmon resonance (SPR) biosensor and did a series of binding assays to determine the relative affinity of Efb-C for C3, hydrolyzed C3 ($C3(H_2O)$), C3b, C3c and C3dg, all of which are known to have distinct conformations and/or ligand-binding properties[23–27] (**Fig. 5a**). Consistent with our isothermal titration calorimetry results (**Fig. 3a**), we found that Efb-C bound to all forms of C3 that included the thioester-containing C3d domain[8]; in contrast, we detected no binding to the C3c fragment.

To expand on those observations, we determined full kinetic profiles for those C3 fragments capable of binding to Efb-C (**Fig. 5b** and **Table 2**). All C3 fragments had affinity constants in the low nanomolar range and, furthermore, these data were internally consistent with our solution calorimetry results (**Fig. 3a**). Nevertheless, the association and dissociation rate constants for each fragment varied considerably. C3dg had a much higher association rate constant than all other C3 analytes, which might be attributed to the unimpeded accessibility of the Efb-C-binding site in this comparatively small fragment. Moreover, even though the dissociation constants of both native C3 and $C3(H_2O)$ were similar, their kinetic profiles were distinct. $C3(H_2O)$ bound Efb-C more quickly, but this complex also dissociated at a rate approximately 1.7-fold greater than the dissociation rate of the complex with native C3 (**Table 2**). Finally, despite the fact that $C3(H_2O)$ has C3b-like functional properties[28], the affinity of Efb-C for C3b was much lower than expected. The affinity of Efb-C for C3b was approximately 70% lower than that of Efb-C for native C3 and was over 90% lower than that of Efb-C for C3dg. Considerable differences in both the association and dissociation rates contributed to the lower affinity. To our knowledge, such a binding preference is unique, as all known complement regulatory proteins bind 'preferentially', if not exclusively, to C3b[2].

We made several observations that provided a potential structural basis for the binding 'preferences' and conformational effects of Efb-C when we interpreted the Efb-C–C3d complex (**Fig. 2**) in the context of the full-length C3 structure[23] (**Fig. 6a**). First, the Efb-C-binding site on C3d includes the H4-H5 and H6-H7 loop regions that adopt altered conformational states during the activation of C3 to $C3(H_2O)$[26] and C3b (J.D.L., unpublished observations), as measured by hydrogen-deuterium–exchange mass spectrometry[29]. Notably, N138 of Efb-C, which was critical for the Efb-C–C3d interaction (**Fig. 2**), made extensive contacts with the H4-H5 loop of the C3d domain. The thermodynamic and kinetic stability of the Efb-C–C3 complex, as determined by both calorimetry and SPR studies (**Figs. 3** and **5**), suggested that the binding of Efb-C to C3 may interfere with movement of the H4-H5 loop to the conformation in the active protein.

Second, in addition to its primary contacts with the C3d domain, as described above, Efb-C seemed poised to make additional interactions with the surface of C3 (**Fig. 6a**, right). In particular, residues V146, M149, V150 and E153 from Efb-C helix α3 were all less than 4 Å from side chains donated by the second α_2-macroglobulin domain of the C3

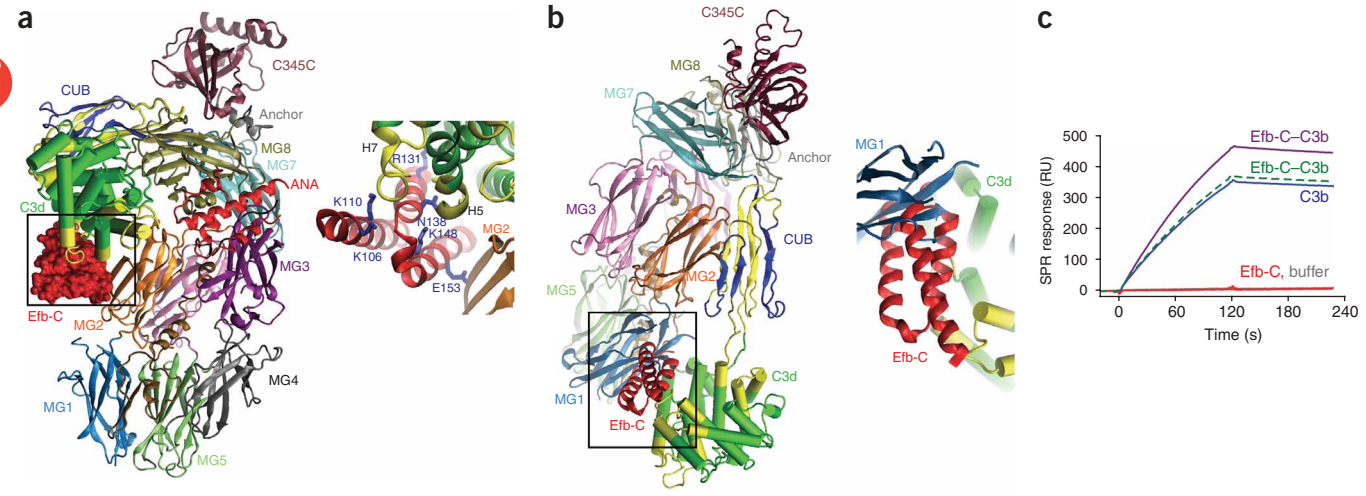

Figure 6 Proposed structural basis for the differential recognition of C3 fragments by Efb-C. (**a**) Localization of Efb-C in the context of native C3 based on the crystal structures of Efb-C–C3d (**Fig. 2**) and C3 (ref. 23). This model has C3 in the same orientation published before[23]. Efb-C, red surface (to avoid confusion with the red ribbon representing the ANA domain of C3a); C3d domain, green tubes; second α_2-macroglobulin domain (MG2), orange; C3 peptides with altered conformations during activation to $C3(H_2O)$, yellow[29]. Right, enlargement of boxed region at left, with Efb-C (red ribbon) and several important side chains (stick models). ANA, anaphylatoxin domain; CUB, C1r-C1s, urinary epidermal growth factor, and bone morphogenetic protein domain. (**b**) Localization of Efb-C (red ribbon) in the context of activated C3b, based on **Figure 2** and the C3b crystal structure[24]. Right, enlargement of boxed region at left. (**c**) Efb-C binding induces a conformational change in C3b. SPR sensorgrams for the binding of C3b (blue line), theoretical Efb-C–C3b (green dashed line), actual Efb-C–C3b (purple line), Efb-C (red line) or buffer alone (gray line) to immobilized antibody C3-9. For clarity, the C3 and C3b color scheme is adapted from a published scheme[23,24].

© 2007 Nature Publishing Group http://www.nature.com/natureimmunology

β-chain. Those additional interactions may well have contributed to the greater affinity of Efb-C for C3 and C3(H_2O) than for C3b, as the crystal structures of C3b have shown that the cognate C3d domain undergoes a translation of 65.7 Å and a rotation of 103.6° relative to its location in C3 (refs. 23,24). The large conformational change that accompanied C3 activation made any additional contacts between Efb-C and the second α_2-macroglobulin domain of C3 physically unlikely (**Fig. 6b** and **Supplementary Fig. 6** online).

We made an equally notable observation when we used the same approach to analyze the Efb-C-binding site in C3b (**Fig. 6b**). Here, Efb-C seemed to undergo a steric 'clash' with the first α_2-macroglobulin domain of the C3b β-chain despite the fact that the C3d domain was relatively more exposed in this structure than in native C3 (refs. 23,24; **Fig. 6b**, right). It is difficult to imagine how such a structure could exist, yet our SPR studies showed that Efb-C formed a stable complex with C3b (**Fig. 5** and **Table 2**). One potential explanation for this interaction is that Efb-C may also induce a structural change in C3b. To test that possibility, we did an SPR binding assay with immobilized monoclonal antibody C3-9 and assessed its reactivity toward C3b and a preformed Efb-C–C3b complex (**Fig. 6c**). The signal intensity for the Efb-C–C3b complex was approximately 30% greater than the anticipated signal calculated from the ideal mass increase of the complex (about 5%), even though C3-9 does not recognize Efb-C. The increased reactivity of the Efb-C–C3b complex relative to C3b alone indicated that the C3-9 epitope became more exposed in the complex and was consistent with the idea that Efb-C binding triggered an additional conformational change in C3b.

DISCUSSION

The most common complement inhibitory strategy used by various pathogens involves the indirect recruitment of host RCA proteins (such as soluble factor H, factor H–like protein 1 or C4b-binding protein) to the bacterial cell surface[30]. Such surface complexes not only retain the complement-inhibitory activities of the host RCA molecules and provide an effective measure of immune evasion but also seem to result in a physical barrier that efficiently separates the bacterial cell surface from the site of the attack[31]. Notably, *S. aureus* seems to have evolved an alternative strategy in which secreted proteins are used directly to block the various steps needed for the initial activation of the complement response. Indeed, identification of the secreted complement inhibitory protein SCIN[9] that seems to function in a way distinct from that of Efb indicates that *S. aureus* has evolved multiple, mechanistically distinct proteins capable of inhibiting the complement system.

Here we have presented a structure of a pathogen-derived protein bound to a component of the complement cascade and have provided evidence for a previously unappreciated mode of complement inhibition. In this mechanism, Efb-C blocks the formation of the functional C3b opsonin by binding tightly to the thioester-containing domain of native C3 and by perturbing the overall solution conformation of the molecule to one that is incapable of being processed into C3b. Notably, and despite the fact that Efb-C bound 'preferentially' to native forms of C3, we also found that Efb-C recognized C3b with high affinity and seemed to induce a conformational change in this activated complement component. Although the chief mechanism of Efb-mediated inhibition seems to be centered on blocking the generation of active C3b, the abundance of C3 in human plasma indicates that any single mechanism of inhibition is unlikely to be totally effective. Therefore, this additional effect on C3b may contribute physiologically to immune evasion by *S. aureus* and is a topic for future investigation. We believe our findings to be unique, and they elucidate more fully the central importance of conformational change in C3 biology, although in this case in the context of host-pathogen interactions.

The established function of Efb as a virulence factor[18] raises the possibility of targeting the Efb-C3 interaction for new anti-staphylococcal compounds, whereas the inhibitory properties of Efb-C also suggest that this protein may be useful either as a natural product or as a template for designing molecules that can be used to block complement activation in clinical settings. Because of the high concentration of C3 in plasma, it is essential that any therapeutic intervention targeting this molecule be very potent. In this respect, Efb-C may be particularly valuable because it features the dual effect of blocking the activation of native C3 as well as perturbing the structure of activated C3b. Despite those properties, the structures presented here show that the Efb-C–C3 interaction is in a relatively discrete, seven-residue region of the Efb-C protein. The existence of a well defined binding site makes this interface a promising starting point for high-throughput screening or for the design of new bioactive peptides, peptidomimetics or other small molecules as therapeutic candidates.

METHODS

Crystallization and structural analysis. The crystallization and X-ray diffraction analysis of Efb-C has been described[32]. After determination of the initial experimental phases to 2.2 Å from selenium multiwavelength anomalous diffraction data with the SOLVE program[33], final experimental phases at the same resolution were calculated with density-modification protocols, and the resultant electron-density maps were used for automated model building with the RESOLVE program[33–35]. An initial atomic model of both Efb-C chains was built into the density-modified 2.2-Å maps (**Table 1**) with the O program[36] and was subjected to a single round of simulated annealing and maximum-likelihood positional refinement with the crystallography and nuclear magnetic resonance system[37] and a native data set processed to a limiting resolution of 1.25 Å (ref. 32). Iterative rounds of model building and water addition were alternated with B-factor and positional refinement, and the final model was attained by translation, liberation and screw rotation refinement with the REFMAC5 program[38,39]. Although the crystallographically unique unit is a dimer, that is not likely to reflect any physiologically relevant formation of oligomers, as Efb-C is a monomer in solution (M.H. and B.V.G. unpublished data). The final model consisted of residues 105–165 in molecule A, residues 106–165 in molecule B and 155 water molecules. No interpretable density was seen for residues 94–104 in molecule A or residues 95–105 in molecule B, and the conformation of the side chains of I105 and R165 in molecule A and I105, K106 and K107 in molecule B could not be interpreted beyond the Cβ positions and were therefore modeled as alanine residues.

Crystals of Efb-C–C3d were grown by vapor diffusion of hanging drops, in which 1 μl of Efb-C–C3d (12 mg/ml) was mixed with 1 μl of 60% (vol/vol) tacsimate, pH 7.0 (Hampton Research), and was equilibrated against a well solution of 60% (vol/vol) tacsimate, pH 7.0 (1 ml). Block-shaped single crystals grew within 3 d in space group $P4_1$ with cell dimensions of a = b = 90.94 Å and c=120.24 Å and two complexes in the asymmetric unit, which corresponded to solvent content of 59%. The structure of Efb-C–C3d was solved by molecular replacement with X-ray diffraction data to a limiting resolution of 2.2 Å collected from a single frozen crystal at SER-CAT Beamline 22-BM of the Advanced Photon Source of Argonne National Laboratory. After data processing with the HKL2000 software package, molecular replacement was done with the refined structure of C3d as a search model (Protein Data Bank accession code, 1C3D; ref. 19) with the MOLREP program[40]. Initial phase improvement was done with solvent flattening by the DM program[40], and stepwise model building, water addition and refinement were accomplished with the O program[36] and crystallography and nuclear magnetic resonance system[37] as described above. The final model was attained after translation, liberation and screw rotation refinement in the REFMAC5 program[38,39] and consists of the vector-encoded sequence GSRST in addition to residues 974–1265 of human C3 and residues 101–165 of Efb-C for both complexes in the asymmetric unit, as well as 281 ordered water molecules. No

© 2007 Nature Publishing Group http://www.nature.com/natureimmunology

interpretable density for residues 94–100 was visible for either molecule of Efb-C in the refined model.

Molecular surfaces and electrostatic field potentials were analyzed and displayed with the GRASP program[41]. Intramolecular distances for protein chains were calculated with the CCP4 suite[40]. Structural superpositions of proteins were done by the local global alignment method with the default parameters[42] (http://as2ts.llnl.gov/). The numbering of both Efb (GenBank accession code, P68799) and human C3 (GenBank accession code, P01024) here reflect sequence positions in the respective pre-proteins. Representations of protein structures were prepared with the VMD software package (http://www.ks.uiuc.edu/Development/).

Complement inhibition assays. The ability of various Efb-derived proteins to inhibit the classical and alternative pathways of complement activation was evaluated with a published enzyme-linked immunosorbent assay (ELISA)–based approach[43,44]. Additional details on the alternative pathway assay are available in the **Supplementary Methods** online.

C3 capture ELISA. EDTA-treated plasma diluted 1:10 in PBS was incubated for 1 h at 37 °C with or without 25 μM Efb-C or Efb-C-(RENE) and was centrifuged for 5 min at 1,460*g*. The supernatant was added to an ELISA plate coated with monoclonal antibody C3-9 (2 μg/ml), which recognizes a neoantigen that is exposed in C3(H_2O), C3b and C3c but not in native C3 (refs. 21,22,45). Wells were washed twice with PBS containing 0.005% (vol/vol) Tween 20 and were incubated with rabbit polyclonal antibody to C3a (2 μg/ml) that had been affinity-purified on a cyanogen bromide–Sepharose column derivatized with an N-terminal C3a peptide (H-SVQLTEKRMDKVGKYP KELRK-NH_2)[45]. Final detection was made with horseradish peroxidase–conjugated goat antibody to rabbit IgG (1:1,000) and ABTS (2,2′-azino-bis(3-ethylbenzothiazoline-6-sulfonic acid) peroxidase substrate by measurement of the absorbance at 405 nm. Values were plotted against the protein concentration and the resulting data set was fit to a logistic dose-response function with Origin 7.0 (OriginLab).

Analytical characterization of Efb-C3 interactions. Detailed methodologies for both the isothermal titration calorimetry and SPR experiments are available in the **Supplementary Methods** online.

Accession codes. Protein Data Bank (refined coordinates and structure factors): Efb-C, 2GOM; Efb-C–C3d, 2GOX.

Note: Supplementary information is available on the Nature Immunology website.

© 2007 Nature Publishing Group http://www.nature.com/natureimmunology

ACKNOWLEDGMENTS

We thank Z. Jin and J. Chrzas of SER-CAT beamlines 22-ID and 22-BM from the Advanced Photon Source of Argonne National Laboratory for technical assistance with diffraction data collection; A. Rux and B. Sachais (University of Pennsylvania) for support with the Biacore 2000; and D. Leahy, S. Bouyain and K. Ramyar for comments during the preparation of this manuscript. C3-9 was provided by C. Erik Hack (Central Laboratory of The Netherlands Red Cross Blood Transfusion Service). Supported by the School of Biological Sciences at the University of Missouri-Kansas City, the University of Missouri Research Board (2509 to B.V.G.) and the National Institute of Allergy and Infectious Diseases (AI30040 to J.D.L.).

AUTHOR CONTRIBUTIONS

M.H. and B.V.G., structural biology and titration calorimetry; G.S., D.R., P.M. and J.D.L., functional assays and SPR.

COMPETING INTERESTS STATEMENT

The authors declare competing financial interests: details accompany the full-text HTML version of the paper at www.nature.com/natureimmunology/.

Published online at http://www.nature.com/natureimmunology
Reprints and permissions information is available online at http://npg.nature.com/reprintsandpermissions

1. *Therapeutic Intervention in the Complement System* (eds. Lambris, J.D. & Holers, V.M.) (Humana, Totowa, New Jersey, 2000).
2. Morikis, D. & Lambris, J.D. *Structural Biology of the Complement System* (eds. Morikis, D. & Lambris, J.D.) (Taylor & Francis, Boca Raton, Florida, 2005).
3. *The Human Complement System in Health and Diseases* (eds. Volanakis, J.E. & Frank, M.) (Marcel Dekker, New York 1998).
4. Patti, J.M., Allen, B.L., McGavin, M.J. & Hook, M. MSCRAMM mediated adherence of microorganisms to host tissues. *Annu. Rev. Microbiol.* **48**, 585–617 (1994).
5. Chavakis, T. *et al. Staphylococcus aureus* extracellular adherence protein serves as anti-inflammatory factor by inhibiting the recruitment of host leukocytes. *Nat. Med.* **8**, 687–693 (2002).
6. Lee, L.Y. *et al.* The *Staphylococcus aureus* Map protein is an immunomodulator that interferes with T cell-mediated responses. *J. Clin. Invest.* **110**, 1461–1471 (2002).
7. Lee, L.Y.L. *et al.* Inhibition of complement activation by a secreted *Staphylococcus aureus* protein. *J. Infect. Dis.* **190**, 571–579 (2004).
8. Lee, L.Y.L., Liang, X., Hook, M. & Brown, E.L. Identification and characterization of the C3 binding domain of the *Staphylococcus aureus* extracellular fibrinogen-binding protein (Efb). *J. Biol. Chem.* **279**, 50710–50716 (2004).
9. Rooijakkers, S.H. *et al.* Immune evasion by a staphylococcal complement inhibitor that acts on C3 convertases. *Nat. Immunol.* **6**, 920–927 (2005).
10. Hornef, M.W., Wick, M.J., Rhen, M. & Normark, S. Bacterial strategies for overcoming host innate and adaptive immune response. *Nat. Immunol.* **3**, 1033–1040 (2002).
11. Sahu, A. & Lambris, J.D. Structure and biology of complement protein 3, a connecting link between innate and acquired immunity. *Immunol. Rev.* **180**, 35–48 (2001).
12. Neth, O., Jack, D.L., Johnson, M., Klein, N.J. & Turner, M.W. Enhancement of complement activation and opsonophagocytosis by complexes of mannose-binding lectin with mannose-binding lectin-associated serine protease after binding to *Staphylococcus aureus*. *J. Immunol.* **169**, 4430–4436 (2002).
13. Kawasaki, A. *et al.* Activation of the human complement cascade by bacterial cell walls, peptidoglycans, water-soluble peptidoglycan components, and synthetic muramylpeptides - studies on active components and structural requirements. *Microbiol. Immunol.* **31**, 551–569 (1987).
14. Bredius, R.G., Driedijk, P.C., Schouten, M.F., Weening, R.S. & Out, T.A. Complement activation by polyclonal immunoglobulin G1 and G2 antibodies against *Staphylococcus aureus*, *Haemophilus influenzae* type B, and tetanus toxoid. *Infect. Immun.* **60**, 4838–4847 (1992).
15. Verbrugh, H.A., Van Dijk, W.C., Peters, R., Van Der Tol, M.E. & Verhoef, J. The role of *Staphylococcus aureus* cell-wall peptidoglycan, teichoic acid, and protein A in the processes of complement activation and opsonization. *Immunology* **37**, 615–621 (1979).
16. Wilkinson, B.J., Kim, Y., Peterson, P.K., Quie, P.G. & Michael, A.F. Activation of complement by cell surface components of *Staphylococcus aureus*. *Infect. Immun.* **20**, 388–392 (1978).
17. Sakiniene, E., Bremell, T. & Tarkowski, A. Complement depletion aggravates *Staphylococcus aureus* septicaemia and septic arthritis. *Clin. Exp. Immunol.* **115**, 95–102 (1999).
18. Palma, M., Nozohoor, S., Schennings, T., Heimdahl, A. & Flock, J.-I. Lack of the extracellular 19-kilodalton fibrinogen-binding protein from *Staphylococcus aureus* decreases virulence in experimental wound infection. *Infect. Immun.* **64**, 5284–5289 (1996).
19. Nagar, B., Jones, R.G., Diefenbach, R.J., Isenman, D.E. & Rini, J.M. X-ray crystal structure of C3d: aC3 fragment and ligand for complement receptor 2. *Science* **280**, 1277–1281 (1998).
20. Harboe, M., Ulvund, G., Vien, L., Fung, M. & Mollnes, T.E. The quantitative role of alternative pathway amplification in classical pathway induced terminal complement activation. *Clin. Exp. Immunol.* **138**, 439–446 (2004).
21. Hack, C.E. *et al.* Disruption of the internal thioester bond in the third component of complement, (C3) which results in the exposure of neodeterminants also present on activation products of C3. An analysis with monoclonal antibodies. *J. Immunol.* **141**, 1602–1609 (1988).
22. Nishida, N., Walz, T. & Springer, T.A. Structural transitions of complement component C3 and its activation products. *Proc. Natl. Acad. Sci. USA* **103**, 19737–19742 (2006).
23. Janssen, B.J.C. *et al.* Structures of complement component C3 provide insights into the function and evolution of immunity. *Nature* **437**, 505–511 (2005).
24. Janssen, B.J., Christodoulidou, A., McCarthy, A., Lambris, J.D. & Gros, P. Structure of C3b reveals conformational changes that underlie complement activity. *Nature* **444**, 213–216 (2006).
25. Isenman, D.E. & Cooper, N.R. The structure and function of the third component of human complement 1. The nature and extent of conformational changes accompanying C3 activation. *Mol. Immunol.* **18**, 331–339 (1981).
26. Isenman, D.E., Kells, D.I.C., Cooper, N.R., Muller-Eberhard, H.J. & Pangburn, M.K. Nucleophilic modification of human complement component protein C3: correlation of conformational changes with acquisition of C3b-like functional properties. *Biochemistry* **20**, 4458–4467 (1981).
27. Isenman, D.E. Conformational changes accompanying proteolytic cleavage of human complement protein C3b by the regulatory enzyme factor I and its cofactor H. Spectroscopic and enzymological studies. *J. Biol. Chem.* **258**, 4238–4244 (1983).
28. Nilsson, B. *et al.* Confomational differences between surface-bound and fluid-phase complement component-C3 fragments. Epitope mapping by cDNA expression. *Biochem. J.* **282**, 715–721 (1992).
29. Winters, M.S., Spellman, D.S. & Lambris, J.D. Solvent accessibility of native and hydrolyzed human complement component 3 analyzed by hydrogen/deuterium exchange and mass spectrometry. *J. Immunol.* **174**, 3469–3474 (2005).
30. Lindahl, G., Sjobring, U. & Johnsson, E. Human complement regulators: a major target for pathogenic microorganisms. *Curr. Opin. Immunol.* **12**, 44–51 (2000).

31. Zipfel, P.F. *et al.* Factor H family proteins: on complement, microbes and human diseases. *Biochem. Soc. Trans.* **30**, 971–978 (2002).
32. Hammel, M., Ramyar, K.X., Spencer, C.T. & Geisbrecht, B.V. Crystallization and X-ray diffraction analysis of the complement component-3 (C3) inhibitory domain of Efb from *Staphylococcus aureus*. *Acta. Cryst. F.* **62**, 285–288 (2006).
33. Terwilliger, T.C. & Berendzen, J. Automated MAD and MIR structure solution. *Acta Crystallogr. D Biol. Crystallogr.* **55**, 849–861 (1999).
34. Terwilliger, T.C. Maximum likelihood density modification. *Acta Crystallogr. D Biol. Crystallogr.* **56**, 965–972 (2000).
35. Terwilliger, T.C. Automated main-chain model-building by template-matching and interative fragment extension. *Acta Crystallogr. D Biol. Crystallogr.* **59**, 34–44 (2002).
36. Jones, T.A., Zou, J.-Y., Cowan, S.W. & Kjeldgaard, M. Improved methods for the building of protein models in electron density maps and the location of errors in the models. *Acta Crystallogr. D Biol. Crystallogr.* **47**, 110–119 (1991).
37. Brunger, A.T. *et al.* Crystallography & NMR system: a new software suite for macromolecular structure determination. *Acta Crystallogr. D Biol. Crystallogr.* **54**, 905–921 (1998).
38. Murshudov, G.N., Lebedev, A., Vagin, A.A., Wilson, K.S. & Dodson, E.J. Efficient anisotropic refinement of macromolecular structures using FFT. *Acta Crystallogr. D Biol. Crystallogr.* **55**, 247–255 (1999).
39. Winn, M., Isupov, M. & Murshudov, G.N. Use of TLS parameters to model anisotropic displacments in macromolecular refinement. *Acta Crystallogr. D Biol. Crystallogr.* **57**, 122–133 (2001).
40. The Collaborative Computational Crystallography Project 4. The CCP4 suite: programs for protein crystallography. *Acta Cryst. D* **50**, 760–763 (1994).
41. Nicholls, A., Sharp, K.A. & Honig, B. Protein folding and association: insights from the interfacial and thermodynamic properties of hydrocarbons. *Proteins* **11**, 281–296 (1991).
42. Zemla, A. LGA: a method for finding 3D similarities in protein structures. *Nucleic Acids Res.* **31**, 3370–3374 (2003).
43. Kraus, D., Medof, D.E. & Mold, C. Complementary recognition of alternative pathway activators by decay-accelerating factor and factor H. *Infect. Immun.* **66**, 399–405 (1998).
44. Sfyroera, G., Katragadda, M., Morikis, D., Isaacs, S.N. & Lambris, J.D. Electrostatic modeling predicts the activities of orthopoxvirus complement control proteins. *J. Immunol.* **174**, 2143–2151 (2005).
45. Becherer, J.D., Alsenz, J., Esparza, I., Hack, C.E. & Lambris, J.D. A segment spanning residues 727–768 of the complement C3 sequence contains a neoantigenic site and accomodates the binding of CR1, factor H, and factor B. *Biochemistry* **31**, 1787–1794 (1992).

© 2007 Nature Publishing Group http://www.nature.com/natureimmunology

Supplementary Figure 1

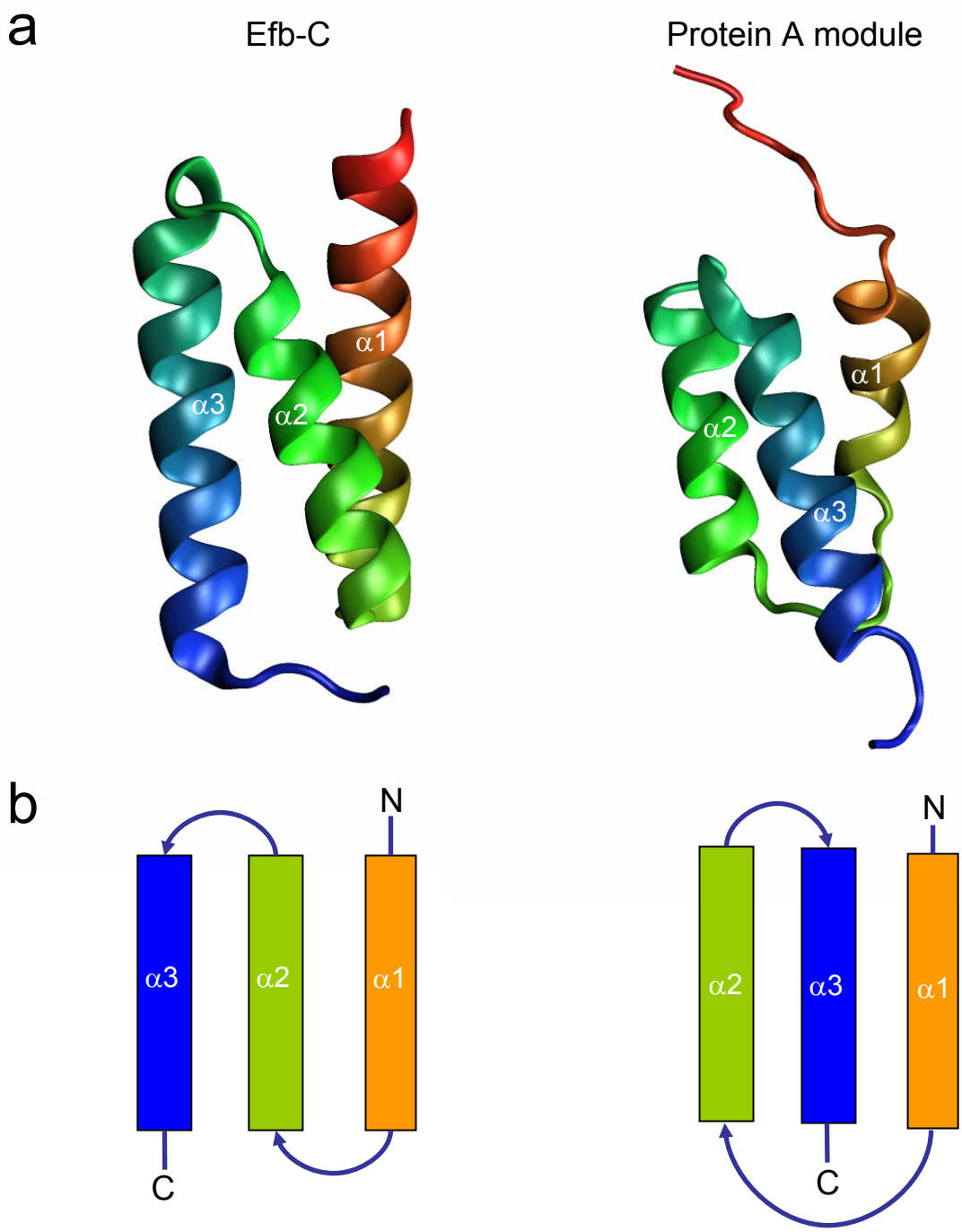

Supplementary Figure 1. Structural comparisons between Efb-C and a protein A module from *S. aureus*. (**a**) Ribbon representation of Efb-C (left panel) and the averaged solution NMR structure of a protein A module from *S. aureus* (RSCB Accession Code 1BDD[1], right panel). Proteins are shown with an indexed color scheme, where the N-terminus appears in red and the C-terminus in blue. The locations of individual helices are indicated. (**b**) Schematic diagrams showing the topological relationships of individual helices in Efb-C (left panel) and protein A modules (right panel).

Supplementary Figure 2

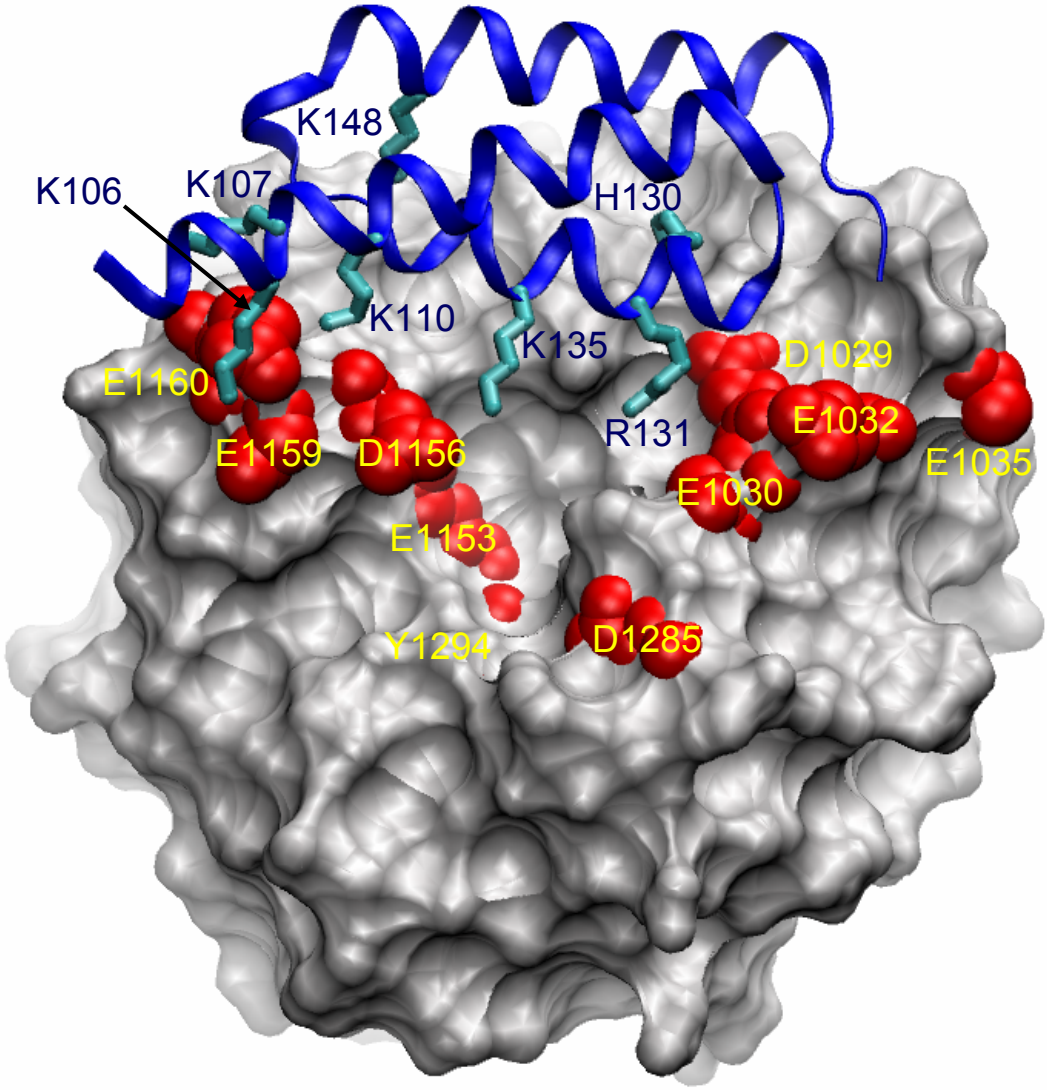

Supplementary Figure 2. Spatial relationship of Efb-C to the conserved acidic groove of C3d as seen in the Efb-C–C3d crystal structure. Efb-C is shown as a blue ribbon, and positively charged residues that contact C3d are drawn as teal sticks. Predominantly acidic, conserved residues that form a negatively charged groove on the C3d surface are shown in red[2]. Efb-C residue positions are indicated in blue, while C3d residue positions are indicated in yellow.

Supplementary Figure 3

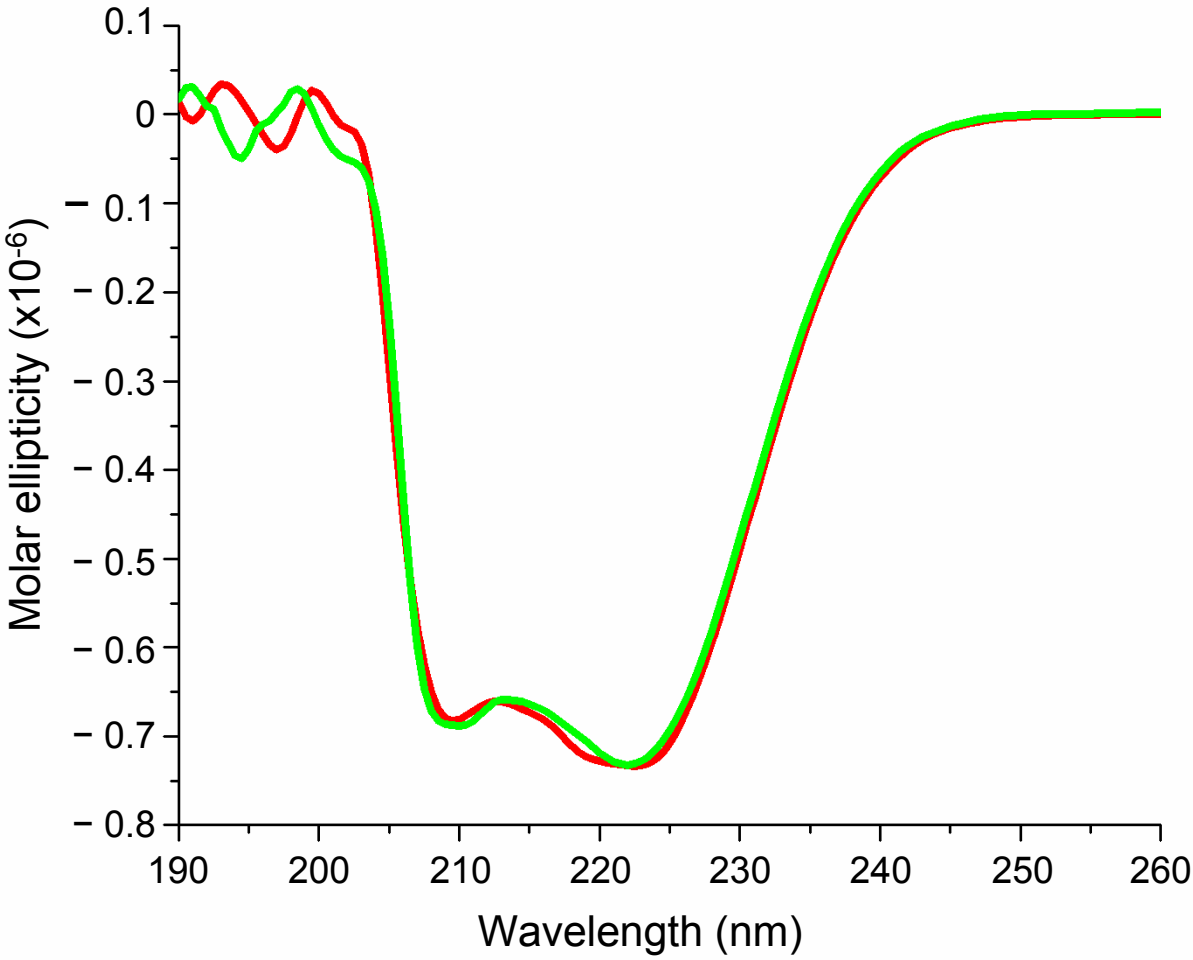

Supplementary Figure 3. Structural integrity of the Efb-C-(RENE) mutant. Circular dichroism spectropolarimetry was used to compare the structural integrity of Efb-C-(RENE) (green trace) with wild-type Efb-C (red trace). The minima observed near 208 and 222 nm in both spectra are characteristic of the α-helical fold adopted by Efb-C.

Supplementary Figure 4

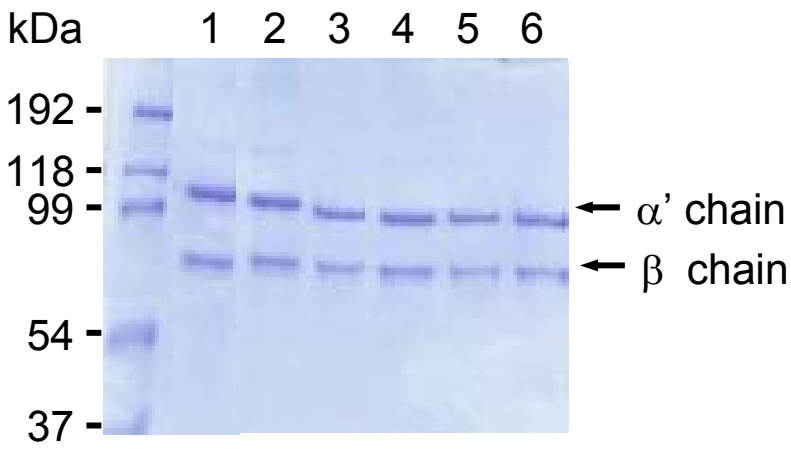

Supplementary Figure 4. Efb-binding renders C3 susceptible to proteolysis *in vitro*. Control digests were performed to ensure the integrity of the proteolysis experiment presented in **Fig. 4** as follows: (1) C3 + trypsin + SBTI, (2) C3b + Efb-C, (3) C3b + Efb-C-(RENE), (4) C3b + trypsin + SBTI, (5) C3 + Efb-C, and (6) C3 + Efb-C-(RENE). The lack of digestion in the absence of trypsin indicates that there is no proteolytic activity intrinsic to the Efb-C protein itself.

Supplementary Figure 5

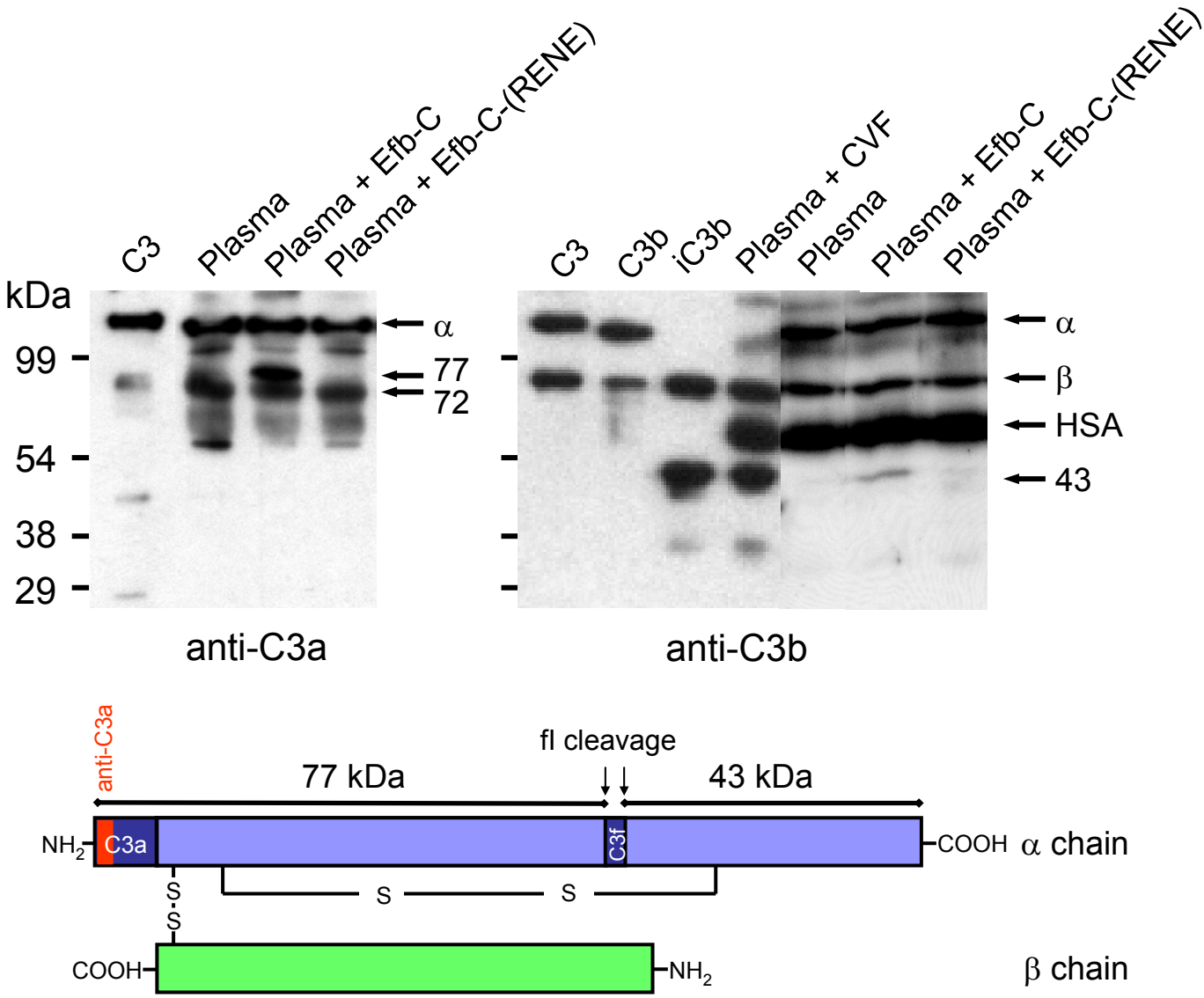

Supplementary Figure 5. Degradation of C3 in complement-inactivated plasma in the presence of Efb-C. The fate of C3 in complement-inactivated plasma was monitored by immunoblot. Diluted EDTA plasma containing either Efb-C, Efb-C-(RENE), or buffer alone was incubated for 2 h at 37 °C. All samples were separated by reducing 9% SDS-PAGE and transferred to PVDF membranes. Immunoblots were probed with either affinity purified rabbit polyclonal anti-C3a or rabbit polyclonal anti-C3b (top panels) and the reactive bands were compared to those of purified C3, C3b, iC3b, and to CVF-treated lepirudin plasma.

Supplementary Figure 6

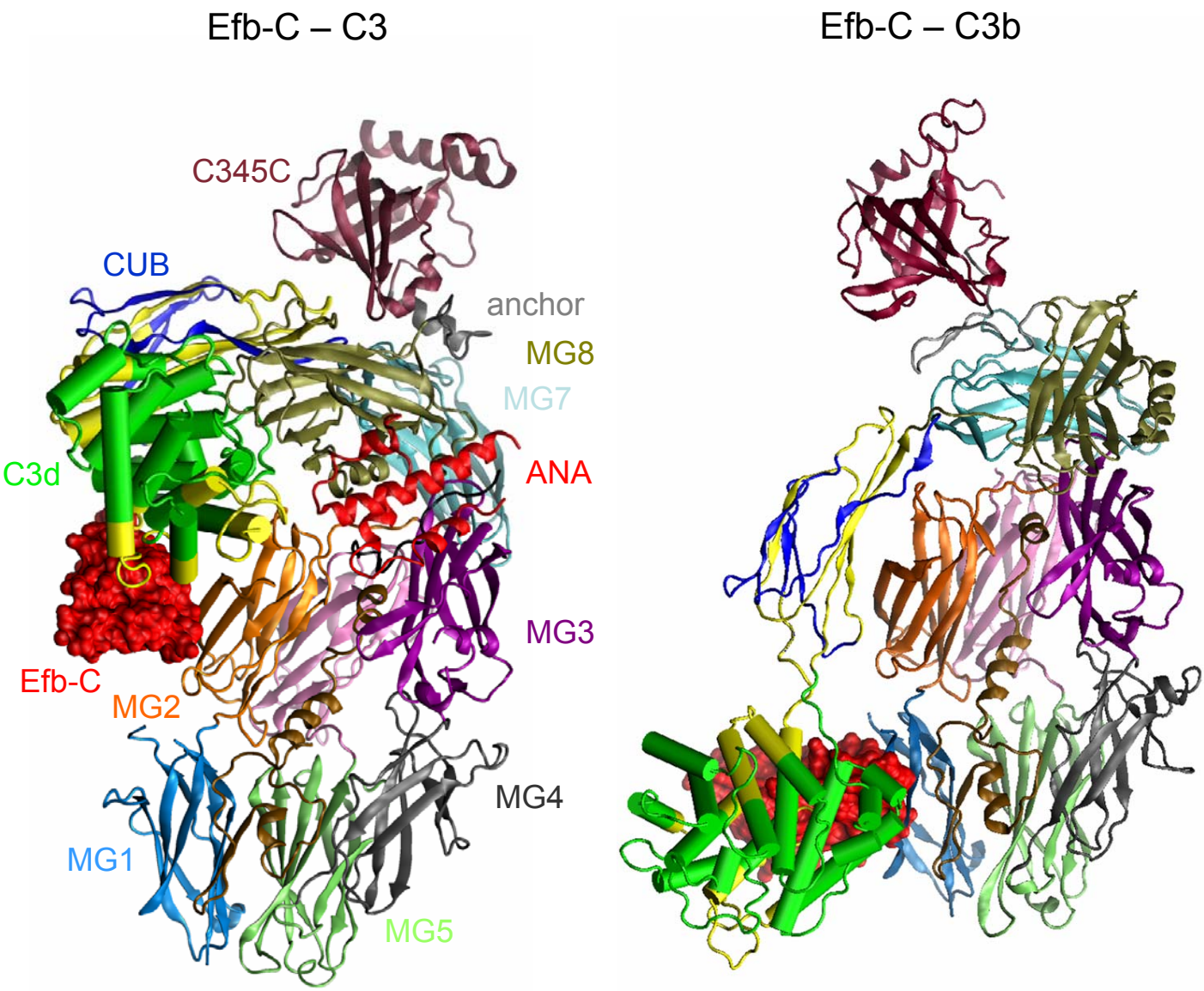

Supplementary Figure 6. Alternative depiction of structural models for Efb-C bound to C3 and C3b. The three dimensional coordinates of C3b3 were superimposed onto those of native C34 by Local-Global Alignment5, and an analogous images to those shown in **Fig. 6** were prepared. The identity of each domain and/or protein is indicated. This view shows the substantial conformational changes associated with activation of native C3 to C3b3, and the relative location of the Efb-C–binding site in each structure.

Supplementary Methods

Degradation of Efb-C-C3 in plasma. Additional bands were visible in Efb-C-treated plasma in both blots presented in **Supplementary Figure 5**. As depicted in the bottom cartoon, the occurrence of a 77 kDa band in the anti-C3a and a 43 kDa band in the anti-C3b blot is indicative of a factor I (fI)-mediated cleavage with removal of the C3f fragment. In contrast, C3a has not been removed as is typically seen during normal degradation of C3 during complement activation. These results indicate that the fI cleavage sites are more exposed in the Efb-C/C3 complex than in native C3, even without cleavage to C3b. However, the intensity of the newly formed bands and the time required for the generation of these bands suggests that this seems not to be the major mechanism of complement inhibition but rather another indication of a conformational change of C3 upon Efb-C binding and the process by which bound C3 is ultimately degraded. Again as it was seen in the purified system (**Figure 4B**), the double mutant Efb-C-(RENE) failed to produce the same degradation pattern seen with the wild type Efb-C. The C3a-specific antibody was affinity-purified using an immobilized N-terminal C3a peptide[6] (indicated by a red bar in the bottom cartoon). The visualization of a 72 kDa band in all plasma samples may be derived from a cross-reactivity of anti-C3a with a protein of unknown nature in the plasma.

Surface plasmon resonance studies. The sensorgrams of C3(H_2O), C3b, and C3d binding to Efb-C were well described by a 1:1 Langmuir binding model, and indicative of a single interaction site for these proteins on Efb-C. Only native C3 showed a small but significant deviation from the Langmuir term, and consequently this sensorgram was analyzed by a surface heterogeneity model. Typically, deviations from an ideal 1:1 curve fit might be derived by immobilization-induced heterogeneities. Since all other

C3 fragments followed a 1:1 binding model, heterogeneity of the immobilized Efb-C was unlikely as source for the observed deviations of native C3 in this case. Instead, a secondary binding site, or conformational adaptations during the binding process are more reasonable explanations. Even though the strong affinity constants required rather harsh regeneration conditions (0.1% SDS), the immobilized Efb-C was found to refold quickly with no substantial loss of activity. As a consequence, repetitive sample injections showed a high reproducibility (data not shown). Since the analysis was carried out at low protein densities and at high flow rates, mass transport limitation was ruled out as a cause for the small deviations. Indeed, inclusion of a mass transport term in the kinetic model did not improve the fit, and higher flow rates did not substantially change the kinetic profile (data not shown).

Supplementary Methods

Protein expression and preparation. A DNA fragment encoding the C-terminal C3-binding domain (residues 94–165) of Efb from *S. aureus* strain Mu50 was amplified from the full-length Efb expression vector pT7HMT-Efb via PCR and used to prepare recombinant Efb-C as described[7]. Site-directed mutations described here were introduced into the pT7HMT-Efb-C expression vector by the two-step megaprimer method[7], and the structural integrity of these purified proteins was validated by circular dichroism spectropolarimetry (**Supplementary Figure 3b**, online, and data not shown) according to a previously reported method[7]. A DNA fragment encoding residues 996 through 1287 of human C3 was amplified via PCR to encode the C1010A mutation and subcloned into a modified form of pET28a which lacked all tags. This vector encodes the additional residues G-S-R-S-T at its N-terminus and the C1010A mutation is necessary to avoid the formation of the reactive thioester bond found in native C3[2, 8]. Protein expression and purification of recombinant C3d was carried out according to the general protocol described by Nagar [2], with the exception that microfluidization was used to lyse the induced cells [7]. To obtain the Efb-C–C3d complex for further structural analysis, purified C3d was incubated with Efb-C for 10 min at room temperature at a molar ratio of Efb-C:C3d of 2:1. Unbound Efb-C was separated by gel filtration chromatography on a Superdex 26/60 column (GE Healthcare), and the purified, reconstituted complex was dialyzed against double-deionized water and concentrated by ultrafiltration to 12 mg/ml total protein (as determined by UV-absorption spectrophotometry). For functional characterization and biosensor binding experiments, purified C3, C3(H_2O), C3b, and C3c were all prepared according to established protocols[9]. Recombinant C3dg was expressed in *E. coli* based on a method described previously.[10]. A pET30 vector containing an S-tag was used instead of a pET11b vector with T7 epitope tag, and no biotinylation signal peptide was included.

Complement inhibition assays. To assess the effects of Efb on the alternative pathway, 96-well ELISA plates were coated with 40 g/ml LPS from *Salmonella typhosa* in PBS for 2 h at room temperature. After coating, wells were blocked with 200 1 of 1% BSA for 1 h, and Efb, Efb-C, or its mutant was serially-diluted in GVB-MgEGTA (veronal-buffered saline, pH 7.4, 5 mM barbital, 145 mM NaCl, 0.1% gelatin, 0.1 M $MgCl_2$, and 0.1 M EGTA) and added to the wells. Human serum in the same buffer at a final concentration of 1:10 was then added to each well and incubated for 1 h. To detect C3b bound to the wells, a 1:1000 dilution of HRP-conjugated anti-human C3 (ICN Cappel) was used. Following extensive washing with PBS containing 0.005% Tween 20, color was developed by adding ABTS peroxidase substrate, and OD was measured at 405 nm. Percent inhibition was plotted against the protein concentration and the resulting data set was fit to a logistic dose-response function using Origin 7.0 software (OriginLab Corporation). IC_{50} values were obtained from the fit parameters that achieved the lowest χ^2 value.

Trypsin sensitivity assay. 10 g of C3 was incubated at 37 °C with 0.1% (w/w) trypsin in the presence of 5.2 M Efb-C, Efb-C-(RENE), or in buffer alone. Samples were collected at 0, 5, 10, 15 and 20 min following initiation of the reaction. Each reaction was quenched with soy bean trypsin inhibitor (SBTI) and the samples were reduced, denatured, and separated by electrophoresis through a 9% SDS-PAGE gel. Protein bands were visualized by Coomassie staining.

Plasma degradation assay. The fate of C3 in human plasma containing either Efb-C, Efb-C-(RENE), or buffer alone was monitored by immunoblotting. Briefly, plasma samples were pretreated with either EDTA (to block complement activation) or lepirudin and were incubated for 2 h at 37 °C with stoichiometric concentrations of either Efb-C, Efb-C-(RENE), buffer alone, or cobra venom factor (CVF) in the case of lepirudin-treated plasma (as a positive control of complement activation). All samples

were separated using 9% SDS-PAGE under reducing conditions and transferred to PVDF membranes. Following blocking with non-fat dry milk (10% (w/v) in PBS), the membrane was probed with either a polyclonal rabbit anti-C3a antibody that had been affinity-purified against the peptide H-SVQLTEKRMDKVGKYPKELRK-NH_2[6], or polyclonal rabbit anti-C3b. Bound antibodies were detected by chemiluminescence following exposure to an HRP-conjugated goat anti-rabbit secondary antibody.

Analytical characterization of Efb-C3 interactions. ITC experiments were performed at 25 °C using a VP-ITC (Microcal) calorimeter. All proteins were dissolved in 20 mM Tris (pH 8.0) and 200 mM NaCl to a final concentration of either 150 μM for *S. aureus* components or 12 μM for recombinant C3d. A preliminary 1 μl injection of the *S. aureus* protein into a solution of C3d was followed by multiple injections of 5 μl at 240 s intervals and the evolved heat was measured. All data were fit using Origin software (OriginLab) using a single binding site model to give the final experimental values for both enthalpy (H) and entropy (–T S) of binding after correcting the observed heat values for the effect of dilution and subtraction of buffer titration baseline values.

All SPR experiments were performed on a Biacore X (ranking) or Biacore 2000 (kinetic profiling) biosensor at 25 ºC using 10 mM PBS-T (10 mM sodium phosphate, pH 7.4, 150 mM NaCl, 0.005% Tween-20) as running buffer. The ranking assay was performed as previously described[11]. Briefly, 600 resonance units (RU) of Efb-C were immobilized on a CM5 sensor chip using amine coupling according to the manufacturer's suggestions. A separate flow cell was only activated and deactivated, and served as reference surface. 200 nM solutions of the C3 fragments were injected for 3 min at a flow rate of 20 μl/min with a dissociation phase of 3 min. The Efb-C surface was regenerated with two consecutive 30 s pulses of 0.1% SDS and re-equilibrated in running buffer for 10 min. For the kinetic SPR studies, to avoid mass transport effects,

Efb-C was immobilized at lower density (200 RU) and the flow rate was kept at 30 µl/ml. C3 fragments were screened as threefold dilution series (67-0.09 nM; 200-0.09 nM for C3b) in running buffer with injection and dissociation phases of 5 and 10 min, respectively. To ensure full reconstitution of the surface after regeneration, the equilibration phase was increased to 30 min. Three buffer blanks were included in each analysis and their average signals were subtracted from the processed sample responses (double referencing)[12]. Data processing and kinetic analysis was performed using Scrubber (version 2.0a, BioLogic Software Pty Ltd) and CLAMP (version XP)[13]. Each data set was globally fitted to either a Langmuir 1:1 interaction model (C3(H_2O), C3b, and C3dg) or a surface heterogeneity model (C3 native) to obtain the association and dissociation rate constants (k_{on} and k_{off}, respectively). The equilibrium dissociation constant (K_d) was calculated from the kinetic parameters as $K_d = k_{off}/k_{on}$. To prevent native C3 from being hydrolyzed, freshly purified plasma C3 was selectively precipitated by dialysis against MES pH 6.0 as described [4] and stored at -80 ºC. Immediately before analysis, the precipitate was reconstituted in running buffer and kept on ice until injection. To verify that the observed SPR signal for native C3 was not generated by contamination with C3(H_2O), Mono-S cation exchange chromatography was used to further purify the experimental protein sample. The content of residual C3(H_2O) was quantified by an ELISA method using the hydrolyzed C3-specific monoclonal antibody C3-9 [6], and was found to be less than 2% of total protein weight. The purified native C3 fraction was desalted into running buffer and injected onto an Efb-C sensor chip, which resulted in a clear binding signal within the expected experimental range. SPR was also used to test for the induction of conformational change in C3b upon binding to Efb-C. In this experiment, 7,000 RU of monoclonal antibody C3-9 were immobilized as described above. Analyte solutions consisting of 50 nM Efb-C, C3b, or a stoichiometric Efb-C–C3b complex were prepared in PBS-T

and injected for a total of 2 min followed by a 2 min dissociation phase and regeneration with 10 mM glycine pH 2.0 for 60 s.

References

1. Gouda, H., Torigoe, H., Saito, A., Sato, M., Arata, Y., and Shimada, I. Three-dimensional Solution Structure of the B Domain of Staphylococcal Protein A: Comparisons of the Solution and Crystal Structures. Biochemistry 31, 9665-9672 (1992).
2. Nagar, B., Jones, R.G., Diefenbach, R.J., Isenman, D.E., and Rini, J.M. X-ray Crystal Structure of C3d: A C3 Fragment and Ligand for Complement Receptor 2. Science 280, 1277-1281 (1998).
3. Janssen, B. J. C., Christodoulidou, A., McCarthy, A., Lambris, J.D., and Gros, P. Structure of C3b Reveals Conformational Changes Underlying Complement Activity. Nature, In Press (2006).
4. Janssen, B. J. C., Huizinga, E.G., Raaijmakers, H.C.A., Roos, A., Daha, M.R., Ekdahl-Nilsson, K., Nilsson, B., and Gros, P. Structures of Complement Component C3 Provide Insights Into the Function and Evolution of Immunity. Nature 437, 505-511 (2005).
5. Zemla, A. LGA: a method for finding 3D similarities in protein structures. Nucleic Acids Research 31, 3370-3374 (2003).
6. Becherer, J. D., Alsenz, J., Esparza, I., Hack, C.E., and Lambris, J.D. A Segment Spanning Residues 727-768 of the Complement C3 Sequence Contains a Neoantigenic Site and Accomodates the Binding of CR1, Factor H, and Factor B. Biochemistry 31, 1787-1794 (1992).
7. Sakar, G., and Sommer, S.S. The "Megaprimer" Method of Site-directed Mutagenesis. *Biotechniques* **8**, 404-407 (1990).
8. Sahu, A., and Lambris, J.D. Structure and Biology of Complement Protein 3, a Connecting Link Between Innate and Acquired Immunity. Immunol. Rev. 180, 35-48 (2001).
9. Sahu, A., Soulika, A., Morikis, D., Spruce, L., Moore, W.T., and Lambris, J.D. Binding Kinetics, Structure-Activity Relationship, and Biotransformation of the Complement Inhibitor Compstatin. J. Immunol. 165, 2491-2499 (2000).
10. Guthridge, J. M., Rakstang, J.K., Young, K.A., Hinshelwood, J., Aslam, M., Robertson, A., Gipson, M.G., Sarrias, M.-R., Moore, W.T., Meagher, M., Karp, D., Lambris, J.D., Perkins, S.J., and Holers, V.M. Structural Studies in Solution of the Recombinant N-Terminal Pair of Short Consensus/Complement Repeat Domains of Complement Receptor Type 2 (CR2/CD21) and Interactions with Its Ligand C3dg. Biochemistry 40, 5931-5941 (2001).
11. Sfyroera, G., Katragadda, M., Morikis, D., Isaacs, S.N., and Lambris, J.D. Electrostatic Modeling Predicts the Activities of Orthopoxvirus Complement Control Proteins. J. Immunol. 174, 2143-2151 (2005).
12. Myszka, D. G. Improving Biosensor Analysis. J. Mol. Recog. 12, 279-284 (1999).
13. Myszka, D. G., and Morton, T.A. CLAMP: a Biosensor Kinetic Data Analysis Program. Trends Biochem. Sci. 23, 149-150 (1998).